fire

MDPI

Article

Fire Endurance of Spherical Concrete Domes Exposed to Standard Fire

Abdelraouf T. Kassem [1], Ayman M. El Ansary [2] and Maged A. Youssef [2,*]

[1] Civil Engineering Department, Beni-Suef University, Beni-Suef 2730401, Egypt; abdelraouf_kassem@eng.bsu.edu.eg
[2] Department of Civil and Environmental Engineering, Western University, London, ON N6A 5B9, Canada; aelansa@uwo.ca
* Correspondence: youssef@uwo.ca

Abstract: Fire is considered a common hazard for civil structures. Public and administrative buildings are commonly designed by considering the standard fire rating and, in many cases, contain large compartments with central domes, in which fire growth can be significant. Moreover, tanks and underground fortified structures may be constructed as domes to support the heavy soil above. This paper numerically addressed such a case. First, an axisymmetric finite element model was developed and validated to predict the dome's transient, thermal, structural, and thermal-structural behavior. Next, the model was used to conduct a parametric study to investigate the effects of the dome ring reinforcement, thickness, stiffness, central angle, base restraints, load type (external pressure or gravitational), and load ratio on the fire endurance of the dome. Design recommendations to increase the fire endurance of concrete domes were formulated based on the parametric study.

Keywords: fire endurance; concrete; spherical domes; thermal-structural analysis; finite element

check for updates

Citation: Kassem, A.T.; El Ansary, A.M.; Youssef, M.A. Fire Endurance of Spherical Concrete Domes Exposed to Standard Fire. *Fire* **2024**, *7*, 208. https://doi.org/10.3390/fire7060208

Academic Editor: Siqi Huo

Received: 30 April 2024
Revised: 11 June 2024
Accepted: 17 June 2024
Published: 19 June 2024

1. Introduction

Figure 1 presents examples of spherical concrete domes. Their aesthetics and large spans make them attractive structural systems for many applications. The photos show the typical geometrical forms: a spherical cap (partial dome) and a semi-sphere (full dome).

Failure of a concrete dome could happen in either the ring or the meridian direction. Failure in the ring direction transforms the dome into several arches balanced at the apex. In contrast, failure in the meridian direction results in instability, leading to a total collapse. Spherical concrete domes are typically reinforced in the ring direction to prevent hoop brittle tensile failure. In contrast, the meridian direction is usually unreinforced or has minimum reinforcement.

(**a**) Partial dome (**b**) Full dome

Figure 1. Spherical dome geometry [1].

Zingoni and Enoma [2] presented a closed-form formulation for both meridian and hoop stresses. Figure 2 shows the typical dome statical system and the developed stresses, where ϕ is the central angle in the meridian direction, θ is the central angle in the ring direction, a is the radius in the meridian direction, h is the supported hydrostatic head, and γ is the fluid unit weight.

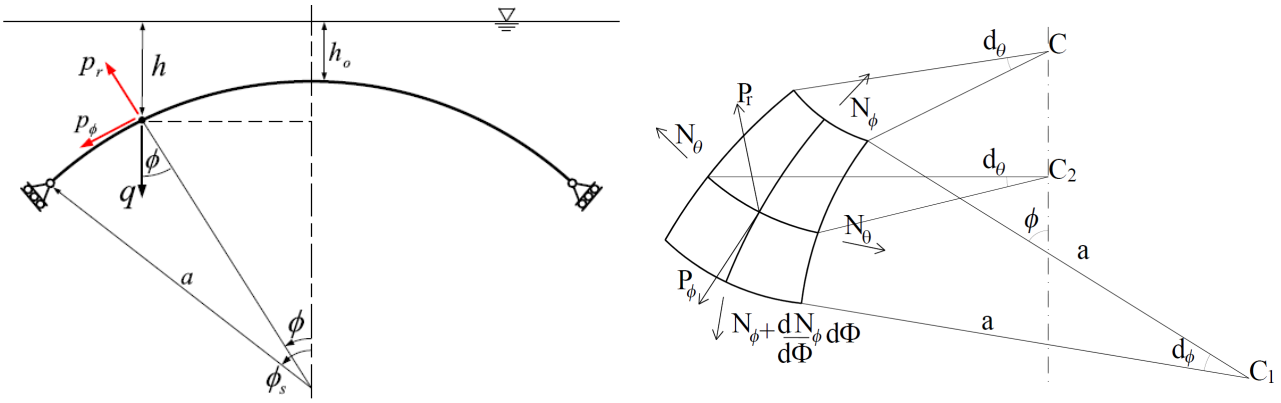

(**a**) Dome statical system (**b**) Dome stresses

Figure 2. Dome loads and stresses [2].

The stresses in the meridian (N_Φ) and ring (N_θ) directions can be evaluated using Equations (1) and (2), considering gravitational loads (q), and Equations (3) and (4), considering pressure loads.

$$N_\Phi = -\frac{qa}{1+cos\varnothing} \tag{1}$$

$$N_\theta = -qa\left[cos\varnothing - \frac{1}{(1+cos\varnothing)}\right] \tag{2}$$

$$N_\Phi = -\frac{\gamma a^2}{6}\left[\frac{1-cos\varnothing}{1+cos\varnothing}(1+2cos\varnothing) + \frac{3h_o}{a}\right] \tag{3}$$

$$N_\theta = -\frac{\gamma a^2}{6}\left[\frac{1-cos\varnothing}{1+cos\varnothing}(5+4cos\varnothing) + \frac{3h_o}{a}\right] \tag{4}$$

Equations (3) and (4) can be simplified for the case of constant pressures P to Equations (5) and (6).

$$N_\Phi = -\frac{Pa}{2} \tag{5}$$

$$N_\theta = -\frac{Pa}{2} \tag{6}$$

The equations imply that domes subjected to gravitational loads experience compressive meridional stresses along the height. In contrast, hoop stresses change from compression to tension at $\Phi = 51.8°$. However, external pressure always results in compressive stresses in both meridian and hoop directions.

Fire is a significant hazard for domes due to material degradation and thermal displacements. The elevated temperatures of an uncontrolled fire, which experiences flashover, significantly deteriorate the structural elements' strength and stiffness [3]. Figure 3 shows that these effects can cause a dome to fail. In a standard fire test, the fire endurance of structural elements is usually expressed in terms of the time to failure. In the case of a realistic fire curve, the endurance can be measured using the equivalent standard fire concept [4].

Figure 3. Collapse of a dome in Jakarta due to fire [5].

The problem of a curved concrete structure subjected to a fire load was introduced in the literature for the case of lined circular concrete tunnels [6], which have a single curvature. When these tunnels are subjected to fire, the prevailing failure mode is concrete crushing rather than tunnel buckling [7]. Moreover, structural collapse has been found to take place at temperatures exceeding 1000 °C [7]. Passive protection is commonly used to increase a tunnel's fire endurance [8].

This research aimed to numerically identify the fire endurance of a spherical concrete dome subjected to either superimposed gravitational loads or external pressure during a standard fire incident. The vulnerabilities of the dome's fire endurance to ring reinforcement, thickness, stiffness, central angle, load type, structural boundary conditions, and load ratio were also assessed. Figure 4 presents the configuration of the research problem, where either an external pressure or a uniformly distributed gravitational load is applied simultaneously with the fire load for a specific type of structural support. The following sections present details about the modeling process and the parametric study.

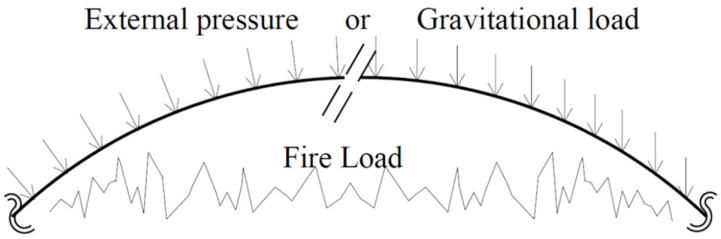

Figure 4. Research problem configuration.

2. Modeling and Validation

Thermal and structural analyses were conducted using Abaqus/CAE 2021 [9]. After examining different modeling techniques, an axisymmetric finite element (FE) model provided good accuracy with reduced computational effort compared to 3D modeling. The model adopted a 4-node deformable CAX4R element [9] for thermal and structural analysis stages.

The transient thermal analysis problem was solved using the Abaqus transient heat transfer module. Recommendations of the Euro code [10] were adopted to determine concrete thermal properties, considering normal-weight siliceous concrete. Average values between the upper and lower limits of concrete thermal conductivity were adopted as a function of temperature. Concrete's specific heat at 0% moisture content was considered as a function of temperature.

The dome's internal air temperature followed the ISO834 fire curve [11]. The air outside the doom was assumed to be at an ambient temperature of 20 °C. The exposed

surface emissivity was set to 0.7 [10], with a convection factor of 25 W/m^{2}K [12], and a value of 10 W/m^{2}K [12] was set for the unexposed surface. Figure 5 shows the FE model and thermal boundary conditions.

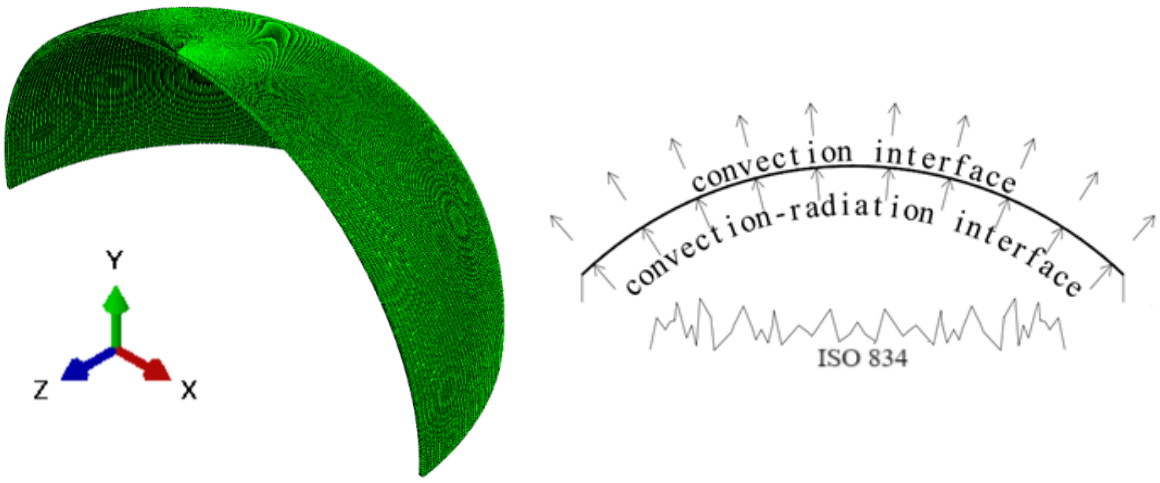

(**a**) FE model configuration (**b**) Thermal boundary conditions

Figure 5. FE geometry for the thermal transient stage.

The number of elements through the dome thickness was determined based on sensitivity analysis. The number of elements through the thickness was varied from 2 to 8, and the temperature profile through the thickness and the apex's vertical deflection were evaluated for each case. Thermal analysis was found to be invulnerable to the number of elements. This invulnerability could be attributed to the adequacy of the element's quadratic shape function in predicting the temperature profile through the dome's thickness. For structural analysis, the vertical deflection indicated that a mesh with four elements through the thickness is optimum. Consequently, the mesh size was varied from 12.5 mm to 50.0 mm.

The thermal model was validated by comparing the average temperatures for a 100 mm thick dome with Kassem's temperature profiles [13]. Figure 6a shows the outputs of the validation model in the form of a temperature distribution through the dome's thickness, while Figure 6b shows the variation in the average dome temperature with time. The model was found to be in good agreement with reference data.

The structural model used the same nodes and elements as the thermal model, which allowed the transient temperatures resulting from thermal analysis to be applied to the structural model. The concrete damage plasticity (CDP) [14] model was used to simulate concrete structural properties [15]. Effects of elevated temperatures on the CDP model were accounted for following Bisby [16], in conjunction with elevated temperature stress–strain parameters, as recommended by the Euro code [10]. The parameters used were a dilation angle (Ψ) of 35°, an eccentricity (e) of 0.1, a ratio of the second stress invariant on the tension meridian to the second stress invariant on the compression meridian (K_c) of 0.67, and a viscosity (μ) of 0.001.

The structural model was validated by examining the thermal expansion and apex deflection under external pressure. The first structural validation model considered a laterally unrestrained 20 m diameter, 100 mm thick dome with all its nodes subjected to a temperature field linearly increasing from 20 °C to 1000 °C in 100 s. Figure 7a shows radial displacements versus the fire duration. The numerically evaluated values matched the theoretical values calculated following the Euro code [10].

The second validation used the experimental work by Chang [17], where a partial concrete dome of diameter 22.63 m and thickness 30 mm was subjected to external pressure. Figure 7b compares the dome's apex vertical deflection predicted numerically to that obtained experimentally by Chang [17]. The structural model slightly underestimated the apex deflection, which might be attributed to the steel ring beam used in the test to support the dome laterally, as it could not provide complete confinement.

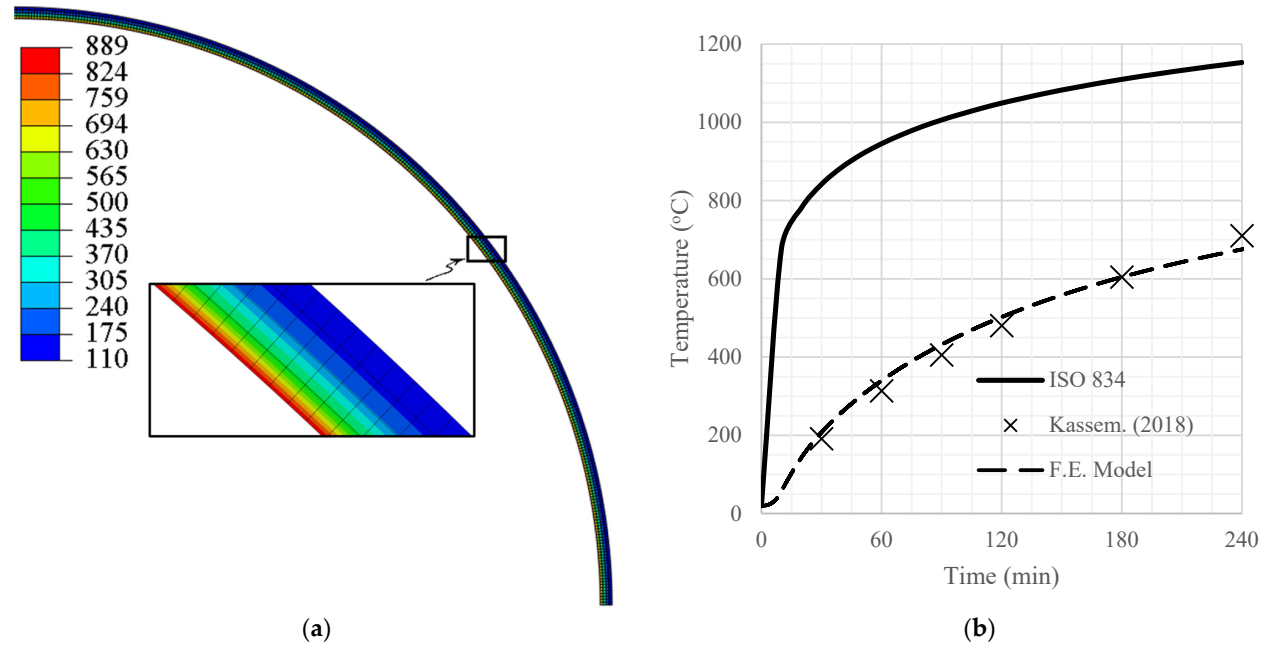

(**a**) (**b**)

Figure 6. Thermal model validation. (**a**) Temperature distribution (°C) after 60 min of ISO834 exposure. (**b**) Thermal model mean temperature [13].

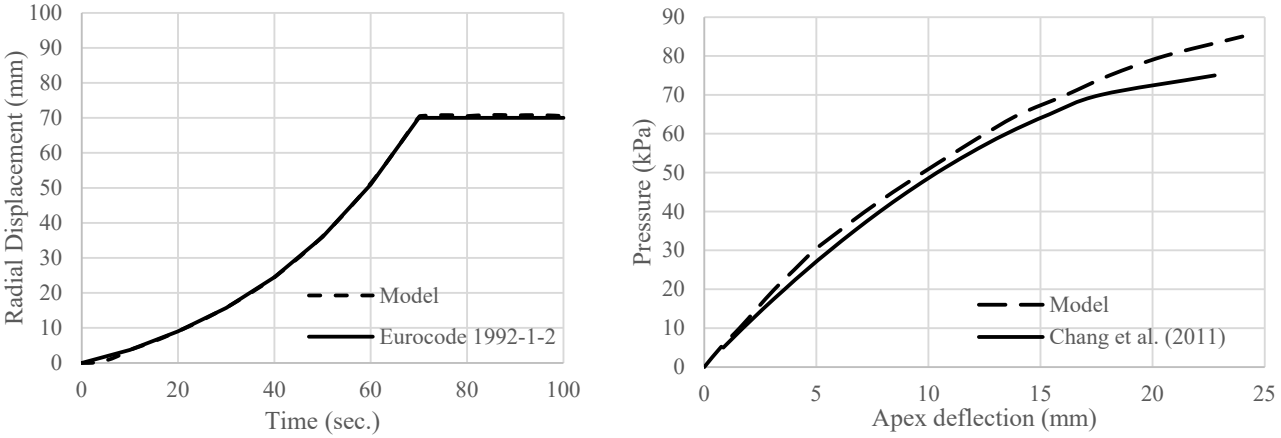

(**a**) Thermal deformations (**b**) Deformations under external pressure

Figure 7. Structural model validation [17].

3. Ring Reinforcement

Ring reinforcement was calculated to prevent ring failure before crushing in the meridian direction. This reinforcement is needed because of the developed ring tension for domes supporting gravitational loads. The maximum ring tension for a full dome is at its base ($\Phi = 90°$), where $\sigma_{meridian} = -qa$ and $\sigma_{hoop} = qa$. The CDP failure criterion is used to identify the needed ring reinforcement. The CDP failure envelope is defined by Equations (7) to (11) [18], where $\overline{F}(\sigma)$ is the material uniaxial compressive strength ($f'c$), $\frac{f_{bo}}{f_{co}}$ is the ratio between the initial biaxial and the uniaxial compressive strengths and $\frac{f_{co}}{f_{to}}$ is the ratio between uniaxial compressive and tensile strengths. For the case of a spherical dome, σ_1 is the meridian stress, and σ_2 is the hoop stress. The meridional direction is considered unreinforced since it is compressed for both gravitational and external pressures. This assumption follows the common practice of using minimum reinforcement in domes to ensure the integrity of the concrete sections. In the case of gravitational loads and for $\Phi > 51.8°$, the concrete tensile strength is ignored in the hoop direction since hoop stresses at failure are far beyond the concrete modulus of rupture. Consequently, the section is

cracked, and only hoop reinforcement resists the tensile forces. Assuming failure in the hoop direction occurs when the steel yields, the behavior in the hoop direction becomes elastic [19], which allows modeling the steel bars as equivalent concrete [20] with a tensile strength of $\frac{A_s}{A_c} f_y$, where $\frac{A_s}{A_c}$ is the reinforcement ratio in the ring direction, and *fy* is the steel yield stress.

$$\overline{F}(\sigma) = \frac{1}{1-\alpha}\left(\sqrt{3J_2} + \alpha I_1 + \beta\sigma_{max}\right) \tag{7}$$

$$I_1 = \sigma_1 + \sigma_2 \tag{8}$$

$$J_2 = \frac{1}{6}\left[(\sigma_1)^2 + (\sigma_1 - \sigma_2)^2 + (\sigma_2)^2\right] \tag{9}$$

$$\alpha = \frac{\left(\frac{f_{bo}}{f_{co}}\right) - 1}{2\left(\frac{f_{bo}}{f_{co}}\right) - 1} \tag{10}$$

$$\beta = (1-\alpha)\frac{f_{co}}{f_{to}} - (1+\alpha) \tag{11}$$

To calculate the needed value of ring reinforcement, different values of $\frac{f_{co}}{f_{to}}$, which reflects the ring reinforcement ratio, were assumed. Assuming $\frac{f_{bo}}{f_{co}}$ = 1.16 [21] and using Equations (7)–(11), the values of $\overline{F}(\sigma)$, σ_1, and σ_2 can be determined. Applying the previous procedure for *f'c* of 30 MPa and *fy* of 400 MPa resulted in Figure 8a, which shows the failure envelopes for different ring reinforcement ratios. The relationship between the meridian reinforcement ratio and hoop stress at failure, i.e., at $\sigma_{meridian} = -\sigma_{hoop}$, is shown in Figure 8b. The figure shows that the rate of increase in the meridian failure stress reduces above a ring reinforcement ratio of about 8%. Assuming this point corresponds to failure in the meridian direction, this ring reinforcement ratio was used in this research.

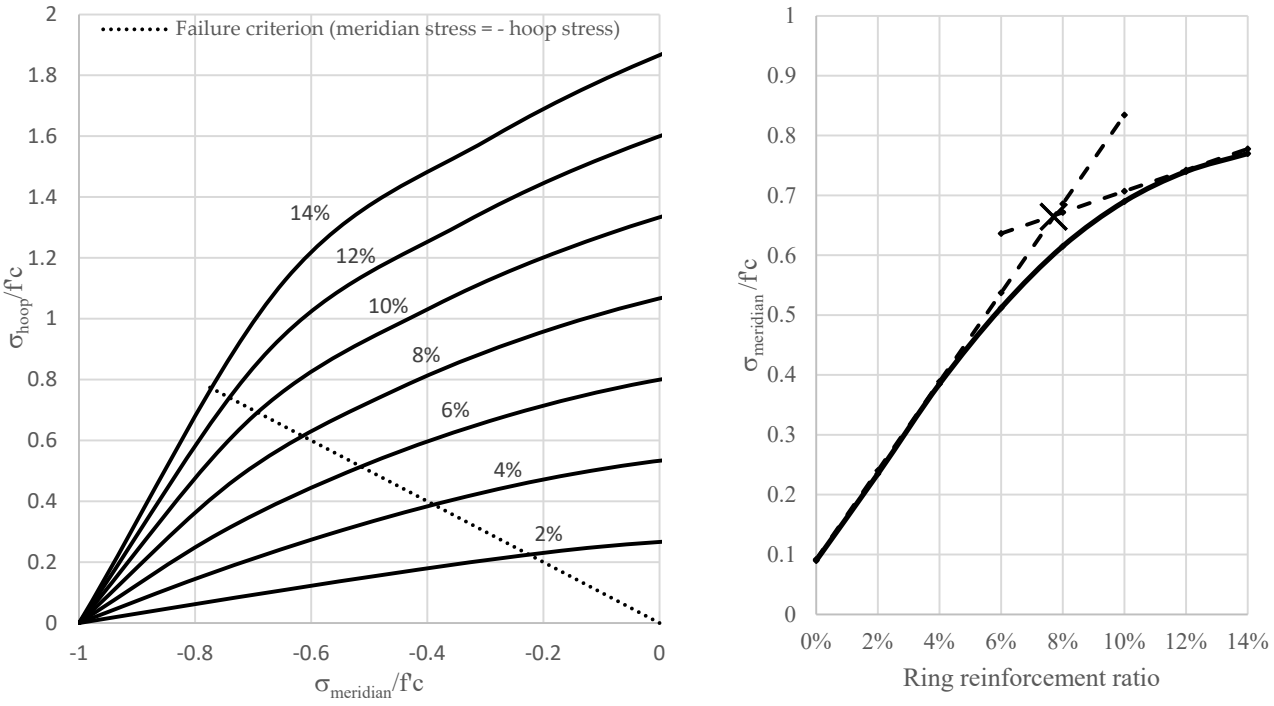

(**a**) Failure envelopes for different ring reinforcement ratios

(**b**) Meridian strength along the failure criterion

Figure 8. Spherical dome biaxial CDP failure criterion.

4. Parametric Study

The vulnerability of the dome's fire endurance to thickness, slenderness, and central angle (partial dome) was examined through a parametric study. Table 1 lists the considered configurations. The configuration name was M, followed by the thickness in centimeters and the diameter in meters. For example, M-10-20 refers to a 100 mm thick dome with a diameter of 20 m. All models had a ring reinforcement ratio of 8% placed in the middle of the thickness of the dome. The influence of the ring reinforcement ratio was assessed by creating two additional models with a ring reinforcement of 0% for high-slenderness-ratio configurations, M-5-20 and M-20-80. Eight models also examined the effects of base restraints and external pressure, considering M-10-5, M-10-10, M-10-20, and M-10-40. The load ratio varied from 30% to 90% of the ambient temperature failure load. The load was applied with standard fire exposure for up to 240 min. This range of the investigated load ratios covers the practical cases in the industry. It ensures that the compressive strain generated in the meridional direction exceeds the tensile strain generated from dome thermal expansion. A concrete characteristic strength of 30 MPa and a steel reinforcement yield strength of 400 MPa were considered for all cases.

Table 1. D/t values for parametric study models.

Thickness t		50 mm	100 mm	200 mm
Diameter D	1.25 m	25 (M-5-1.25)	-	-
	2.50 m	50 (M-5-2.5)	-	-
	5.00 m	100 (M-5-5)	50 (M-10-5)	25 (M-20-5)
	10.0 m	200 (M-5-10)	100 (M-10-10)	50 (M-20-10)
	20.0 m	400 (M-5-20)	200 (M-10-20)	100 (M-20-20)
	40.0 m	-	400 (M-10-40)	200 (M-20-40)
	80.0 m	-	-	400 (M-20-80)

The three considered thicknesses were within the practical range for concrete domes. Figure 9 displays the transient temperatures of the inner (exposed), the mid-thickness, and the outer (unexposed) surfaces, considering exposure to ISO standard fire. The exposed surface temperature remained unchanged regardless of the dome thickness. However, the temperatures at the middle of the thickness and the outer surface were much higher for thinner domes.

The outcomes of the thermal analysis were extracted in the form of nodal temperatures and applied to the structural model. Figure 10 shows the structural model configuration for the cases of full and partial domes, considering both gravitational and pressure loads and transient thermal temperature profiles. The lower boundary condition was set as either fixed to simulate a fully restrained dome or guided to simulate a laterally unrestrained case.

Figure 11 shows the effect of ring reinforcement on the fire endurance of concrete domes subjected to different gravitational load ratios. A 0 or 8 was added to the configuration name to identify the reinforcement ratio percentage. The 0% ring reinforcement ratio showed low fire endurance and invulnerability to the load ratio. The invulnerability could be attributed to a tensile failure in the ring direction shortly after fire exposure. For domes with ring reinforcement, failure in the ring direction was prevented. Thus, the dome fully used its concrete, and the behavior was controlled by the compression happening in the meridian direction.

Figures 12 and 13 represent the effects of dome thickness on fire endurance for slenderness ratios (D/t) of 50 and 200. The figures show that the thicker the dome, the greater the fire endurance. This increase in fire endurance is related to the reduced concrete mean temperature for thicker domes. Consequently, there is less concrete degradation.

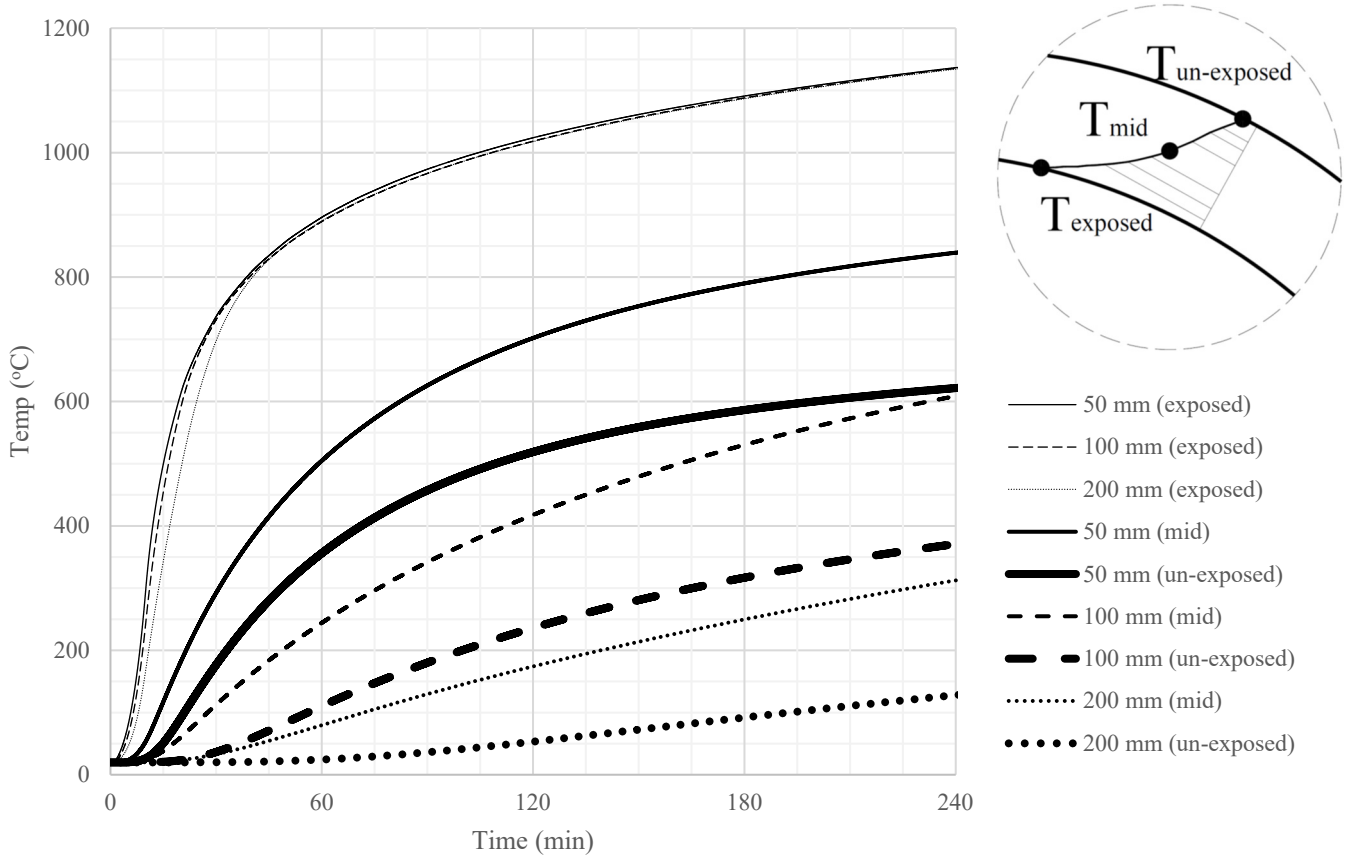

Figure 9. Temperature distribution for domes of various thicknesses subjected to ISO standard fire.

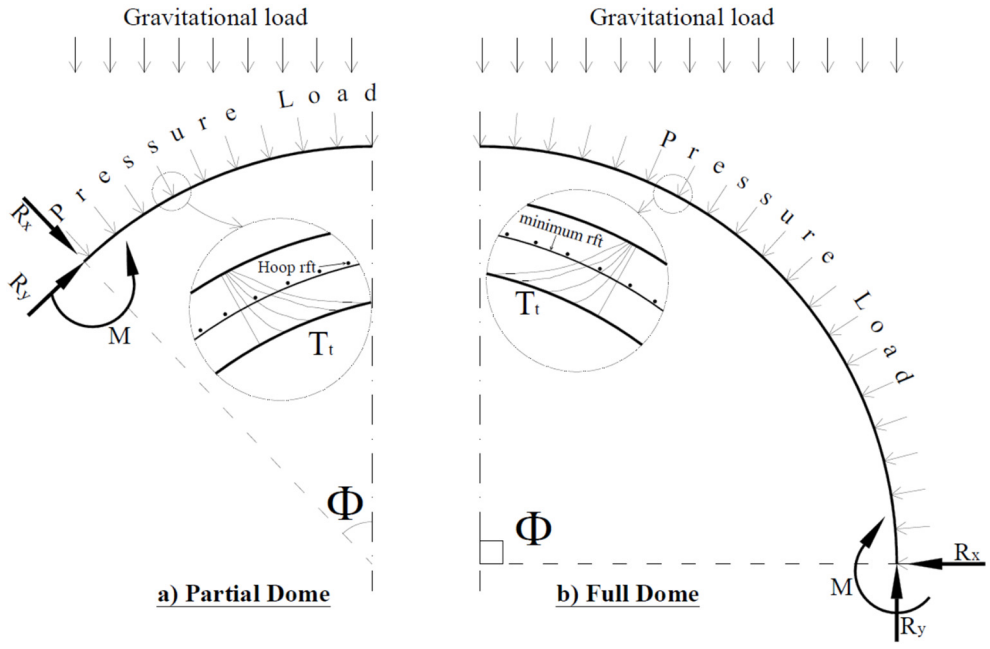

Figure 10. Dome structural model.

Figure 14 represents the direct effect of dome thickness on fire endurance for typical design load ratios (40% to 60%). For a load ratio of 40% and D/t of 100, failure did not happen within the assumed 240 min of fire exposure. The figure shows that fire endurance significantly increases as the thickness increases. It also indicates that domes with a thickness of 50 mm have a fire endurance of less than 60 min.

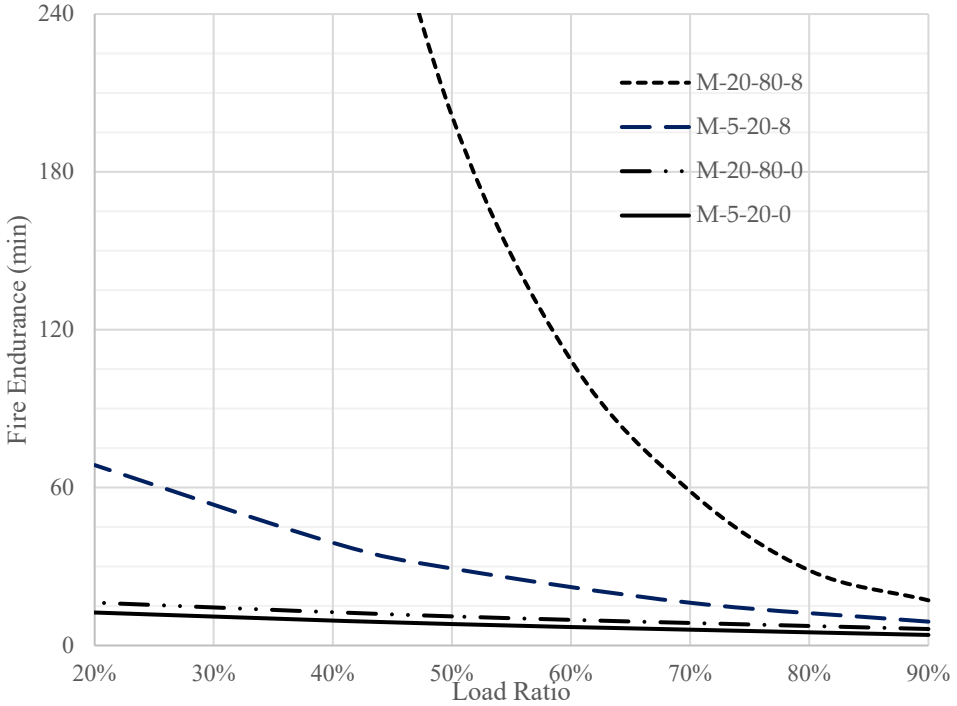

Figure 11. Effect of ring reinforcement on fire endurance.

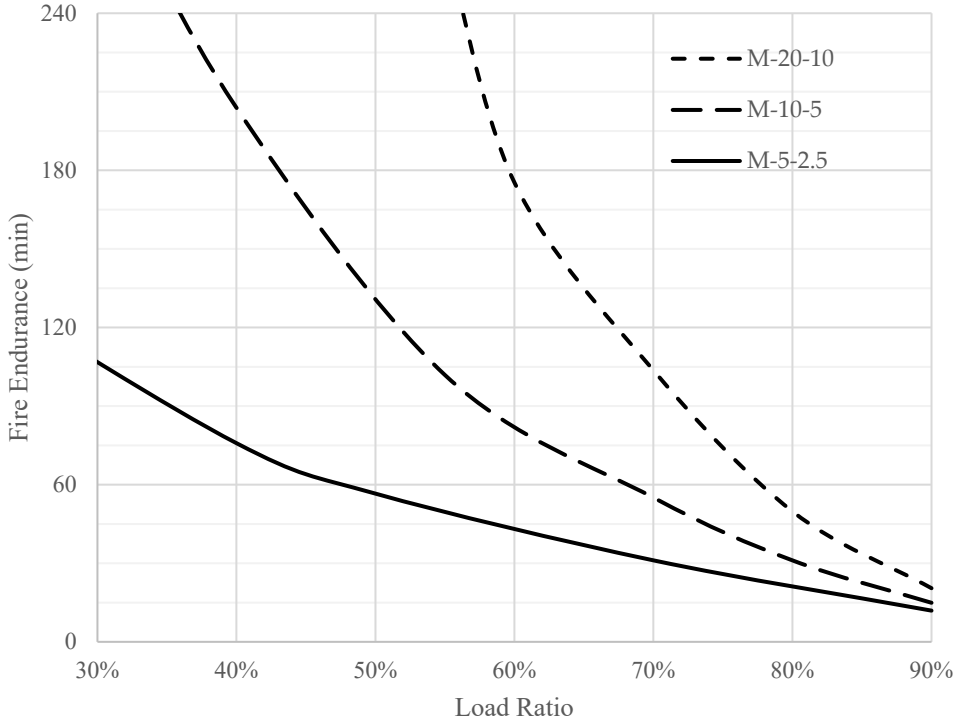

Figure 12. Fire endurance of full domes of D/t = 50 subjected to gravitational load.

The effect of the slenderness ratio on the fire endurance of full domes was investigated, as shown in Figures 15 and 16. The figures clearly show that more slenderness leads to less fire endurance. This observation can be explained by the excessive rotations resulting from the steep temperature gradient in thin domes. However, the fire endurance of domes with low slenderness ratios is approximately the same.

Figure 17a represents the effect of dome stiffness on fire endurance within typical design load ratios (40% to 60%) for a 50 mm thick dome. It shows a reduction in the effect of the load ratio as the slenderness ratio increases, reflecting the role of stiffness in maintaining

membrane action, where domes of high slenderness suffer rotational instabilities and consequently fail at a low fire endurance, as presented in Figure 17b.

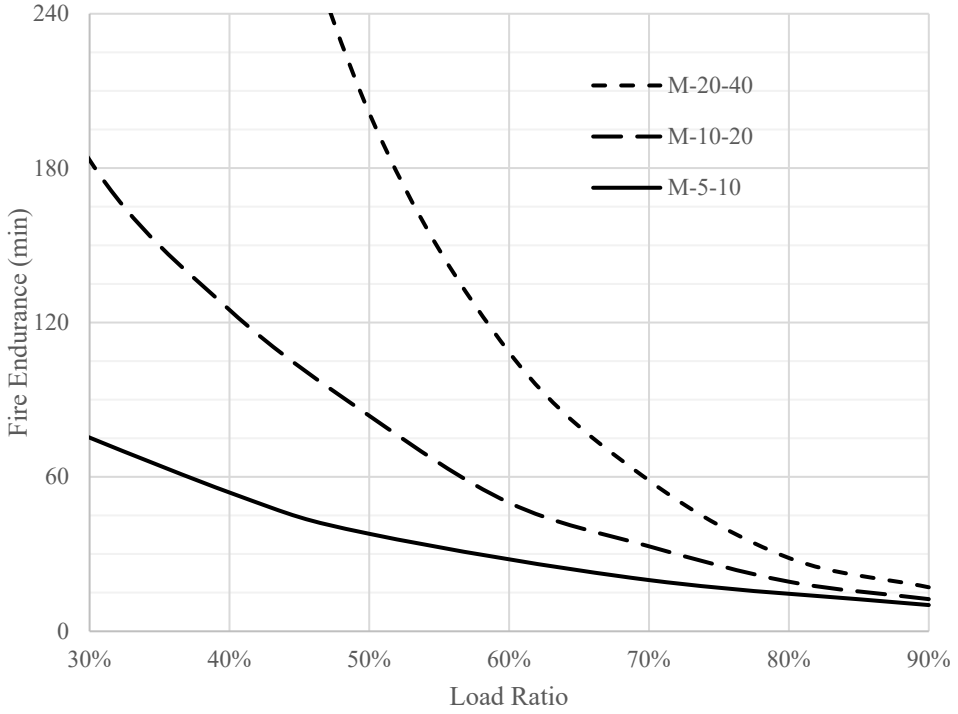

Figure 13. Fire endurance of full domes of D/t = 200 subjected to gravitational load.

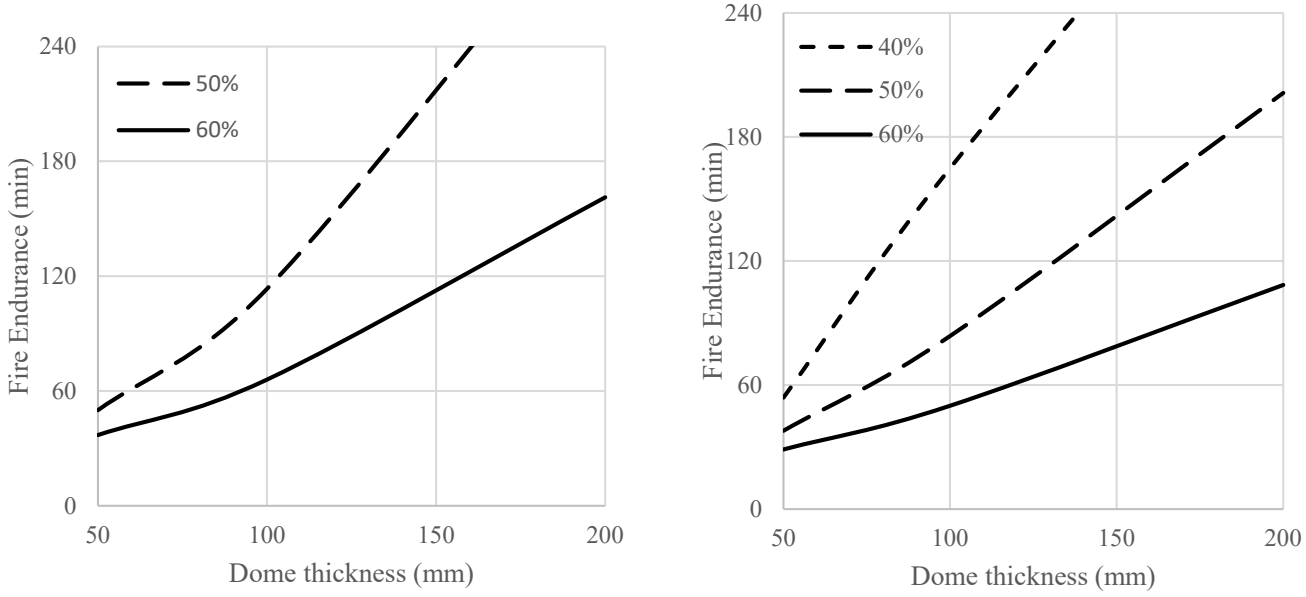

(**a**) D/t = 100 (**b**) D/t = 200

Figure 14. Fire endurance versus dome thickness at common design load ratios.

The behavior of partial domes was considered by modeling a partial dome with a central angle Φ of 40°. This angle is less than 51.8°, ensuring compressive hoop stress. Figure 18 shows that the fire endurance of partial domes (labeled T in the figure caption) is significantly less than that of full domes of the same curvature, which can be attributed to the development of flexure stresses resulting from the base reaction.

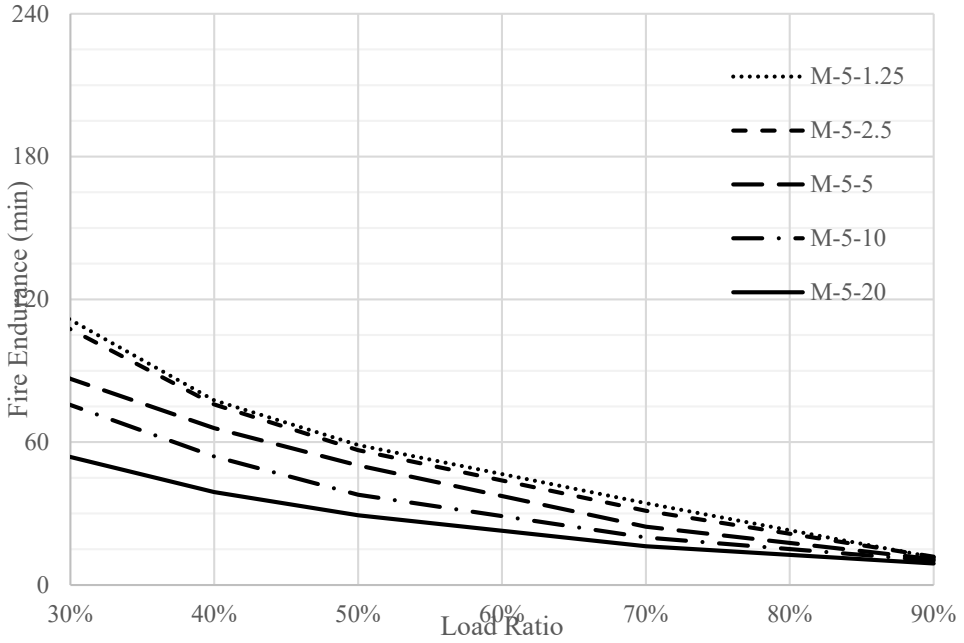

Figure 15. Fire endurance of full domes of thickness 50 mm and various D/t ratios subjected to gravitational load.

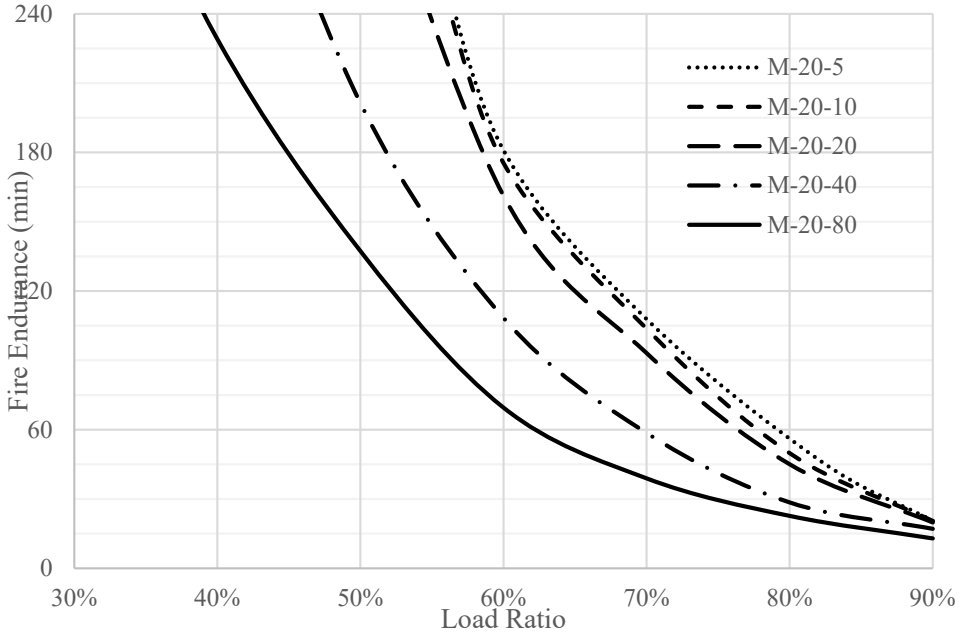

Figure 16. Fire endurance of full domes of thickness 200 mm and various D/t ratios subjected to gravitational load.

Figure 19a shows that laterally unrestrained domes subjected to pressure (P) show no significant decrease in fire endurance for a slenderness ratio exceeding (D/t) = 200. The pressure led to uniform ring compression, stabilizing the slender dome and increasing fire endurance. Laterally restrained full domes (PR) had higher fire endurance than laterally unrestrained full domes (P), as the lateral restraint reaction resulting from thermal expansion provided additional confinement for the dome.

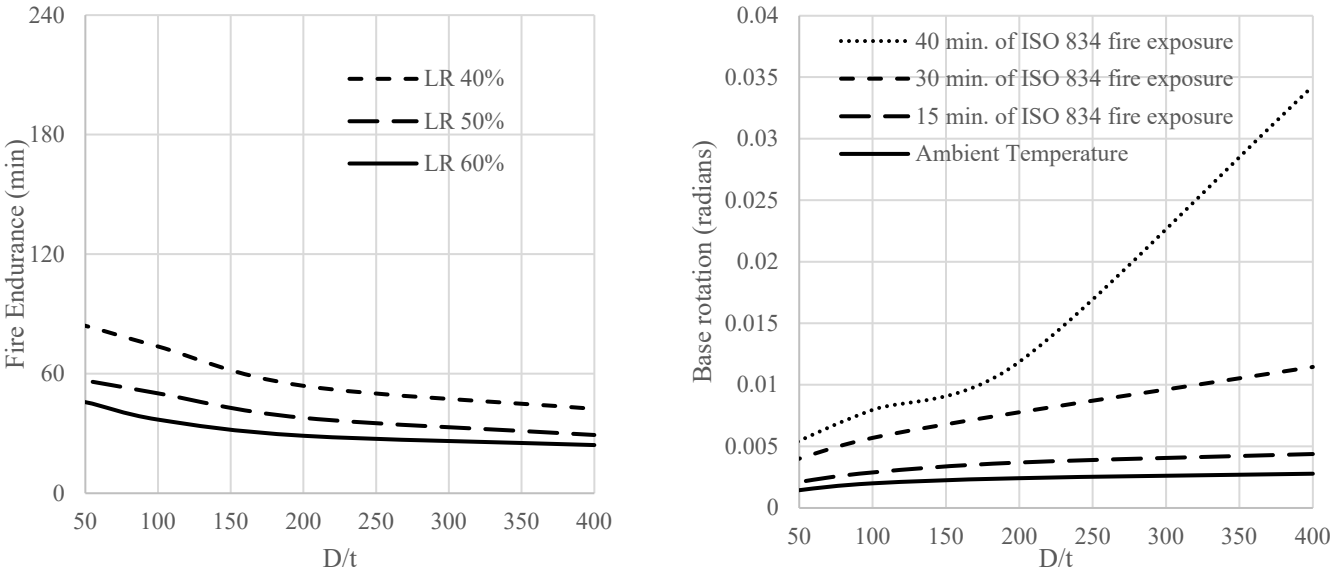

(**a**) Fire endurance for typical design load ratios (**b**) Base rotation for a 40% load ratio

Figure 17. Effect of slenderness on the behavior of domes of 50 mm thickness for various load ratios.

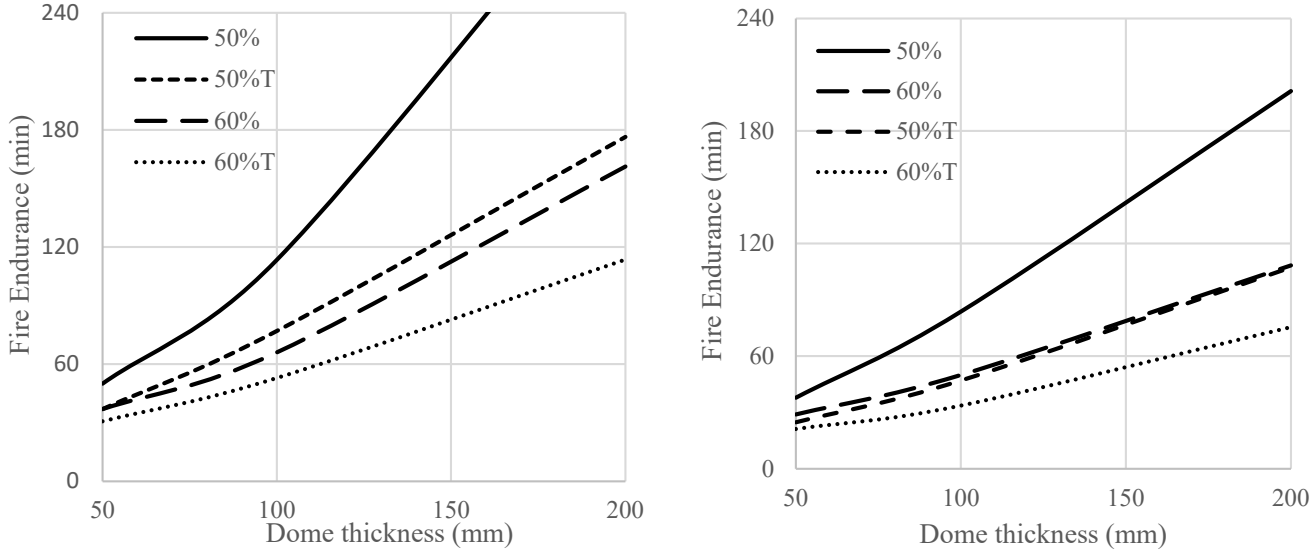

(**a**) D/t = 100 (**b**) D/t = 200

Figure 18. Fire endurance of full and truncated domes of the same curvature (D/t).

Figure 19b shows that laterally restrained full domes subjected to gravitational loads (GR) showed less fire endurance than laterally unrestrained (G) ones, mainly due to the orthogonality of gravitational loads and the lateral restraint reaction. This orthogonality led to flexural deformations, decreasing fire endurance. Figure 20 compares the lateral restraint effects on domes subjected to a fire incident associated with gravitational or external pressure loads. The figure presents a simple illustration of the experienced thermal-structural deformations, considering fixed and guided boundary conditions.

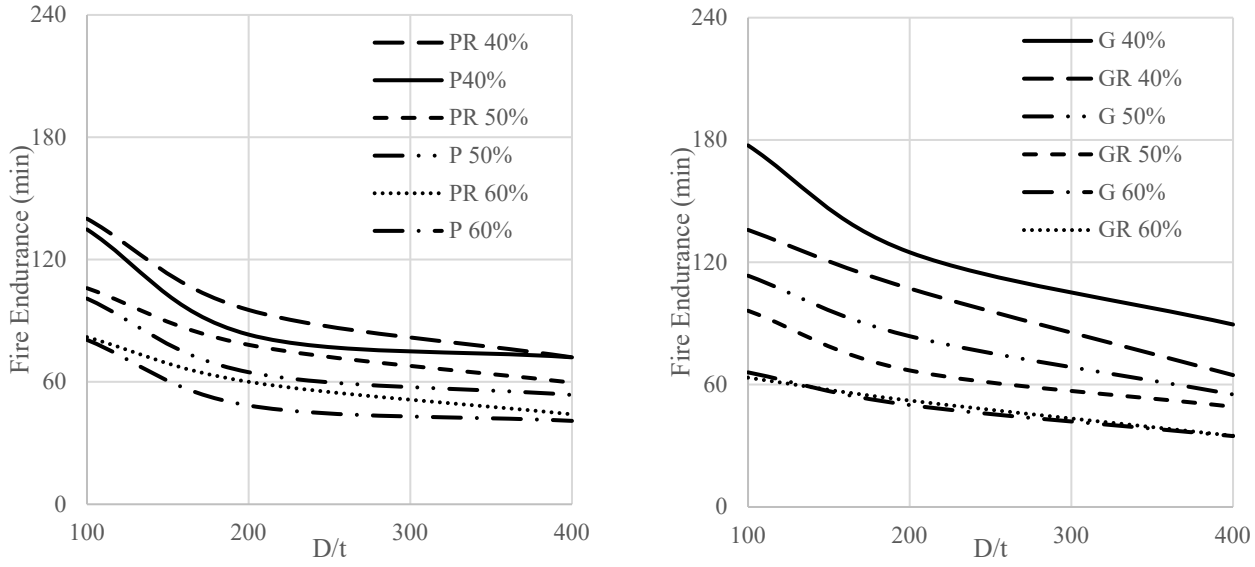

(**a**) External pressure (**b**) Gravitational load

Figure 19. Fire endurance of laterally restrained and unrestrained domes considering different load ratios.

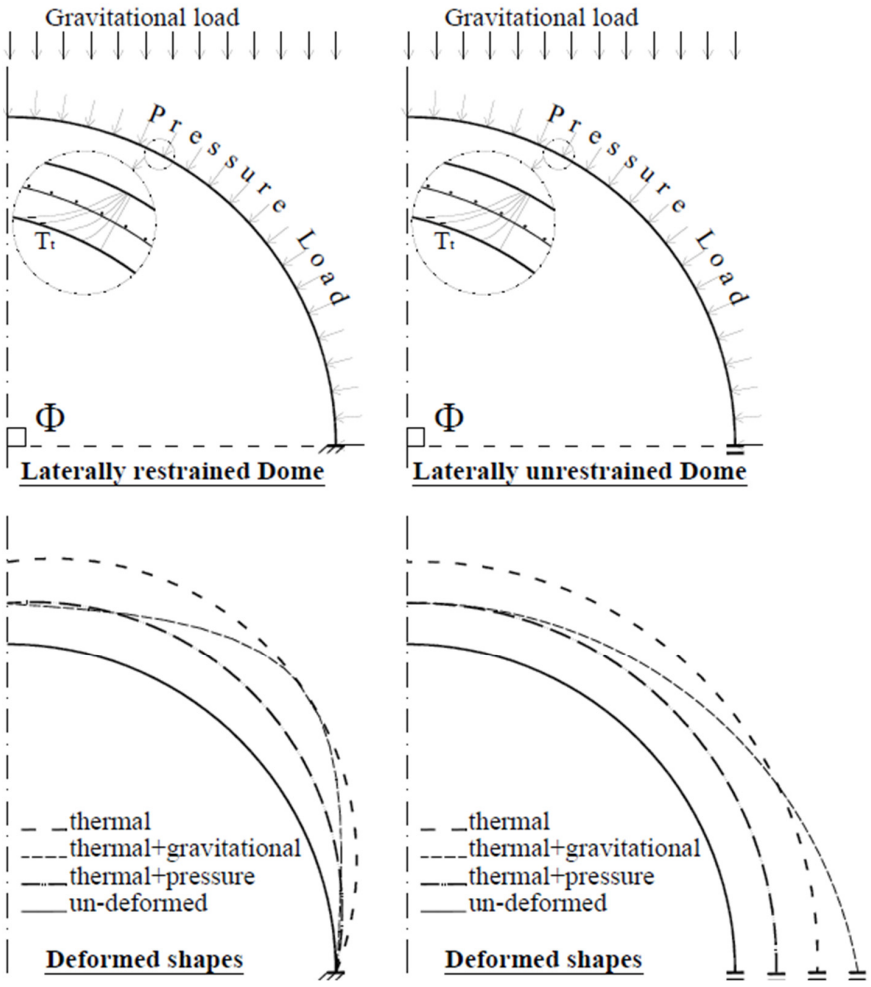

Figure 20. Deformed shapes of laterally restrained and unrestrained full domes subjected to thermal, pressure, and gravitational loads.

5. Conclusions

This comprehensive study examined the behavior of concrete domes subjected to a standard fire incident while supporting gravitational or pressure loads. An axisymmetric finite element model was developed, validated, and used to conduct a parametric study that led to the following conclusions:

- The absence of ring reinforcement leads to early failure during a fire due to ring tensile failure, which makes the failure independent of the value of the applied load. For a concrete strength of 30 MPa and a steel yield strength of 400 MPa, a ring reinforcement ratio of 8% was found adequate to shift the failure to compression in the meridian direction.
- Increasing the thickness of the dome increases the fire resistance and highlights the role of ring reinforcement. It also enlarges the effect of the load ratio on fire endurance.
- Increasing the slenderness ratio reduces the effect of the load ratio on fire endurance as failure becomes controlled by excessive rotations.
- Decreasing the load ratio leads to prolonged nonlinear behavior during fire exposure.
- The fire endurance of full domes is higher than that of partial domes of the same curvature. The difference in fire endurance further increases with an increase in thickness and a decrease in stiffness.
- Lateral restraint increases the fire endurance of domes subjected to an external pressure load. However, it reduces the fire endurance of domes subjected to a gravitational load.
- Fully confined full domes of thickness not less than 100 mm, a slenderness ratio of not more than 100, and a load ratio of not more than 40% could sustain a standard fire for more than two hours without collapsing.
- It is essential that future research investigate and compare the structural integrity of concrete domes subjected to ventilation-controlled fire and identify similarities with and differences from concrete tunnels.

Author Contributions: Conceptualization, A.T.K., A.M.E.A. and M.A.Y.; methodology, A.T.K., A.M.E.A. and M.A.Y.; validation, A.T.K.; formal analysis, A.T.K.; investigation, A.T.K., A.M.E.A. and M.A.Y.; resources, M.A.Y.; data curation, A.T.K., A.M.E.A. and M.A.Y.; writing—original draft preparation, A.T.K.; writing—review and editing, A.M.E.A. and M.A.Y.; visualization, A.T.K.; project administration, M.A.Y.; funding acquisition, M.A.Y. All authors have read and agreed to the published version of the manuscript.

Funding: The authors gratefully acknowledge funding from the Natural Sciences and Engineering Research Council of Canada (NSERC).

Institutional Review Board Statement: Not applicable.

Informed Consent Statement: Not applicable.

Data Availability Statement: The authors confirm that the data supporting the findings of this study are available within the article.

Conflicts of Interest: The authors declare no known competing financial interests or personal relationships that could have influenced the work reported in this paper.

References

1. World Domes. Available online: https://domes.com/projects/ (accessed on 29 April 2024).
2. Zingoni, A.; Enoma, N. Dual-purpose concrete domes: A strategy for the revival of thin concrete shell roofs. *Structures* **2020**, *28*, 2686–2703. [CrossRef]
3. Buchanan, H.; Anthony, K. *Structural Design for Fire Safety*, 2nd ed.; Wiley & Sons: West Sussex, UK, 2001.
4. Fu, F. *Fire Safety Design for Tall Buildings*, 1st ed.; CRC Press: Boca Raton, FL, USA, 2021.
5. The National News. Available online: https://www.thenationalnews.com/world/asia/2022/10/20/watch-giant-dome-collapse-after-indonesia-mosque-fire/ (accessed on 29 April 2024).
6. Hua, N.; Tessari, A.; Khorasani, N.E. Characterizing damage to a concrete liner during a tunnel fire. *Tunn. Undergr. Space Technol.* **2021**, *109*, 103761. [CrossRef]
7. De Silva, D.; Andreini, M.; Bilotta, A.; De Rosa, G.; La Mendola, S.; Nigro, E.; Rios, O. Structural safety assessment of concrete tunnel lining subjected to fire. *Fire Saf. J.* **2022**, *134*, 103697. [CrossRef]

8. Maraveas, C.; Vrakas, A. Design of concrete tunnel linings for fire safety. *Struct. Eng. Int.* **2014**, *24*, 319–329. [CrossRef]
9. Dassault Systemes Simulia Corp. *ABAQUS/Standard User's Manual*; Abaqus/CAE: Providence, RI, USA, 2021.
10. *EN1992-1-2*; Eurocode 2. Design of Concrete Structures—Part 1–2: General Rules—Structural Fire Design. European Standard; CEN: Brussels, Belgium, 2013. Available online: https://www.phd.eng.br/wp-content/uploads/2015/12/en.1992.1.2.2004.pdf (accessed on 29 April 2024).
11. *EN1991-1-2*; Eurocode 1. Actions on Structures—Part 1–2: General Actions—Actions on Structures Exposed to Fire. European Standard; CEN: Brussels, Belgium, 2013. Available online: https://www.phd.eng.br/wp-content/uploads/2015/12/en.1991.1.2.2002.pdf (accessed on 29 April 2024).
12. Kassem, A.T. Buckling of Radially Loaded Concrete Cylinders in Fire Condition. *Civ. Eng. J.* **2019**, *5*, 1214–1226. [CrossRef]
13. Kassem, A.T. Deformations of R.C. Circular Slabs in Fire Condition. *Civ. Eng. J.* **2018**, *4*, 712–723. [CrossRef]
14. Cuong-Le, T.; Le Minh, H.; Sang-To, T. A nonlinear concrete damaged plasticity model for simulation reinforced concrete structures using ABAQUS. *Fratt. Integr. Strutt.* **2022**, *59*, 232–242. [CrossRef]
15. Thienel, K.-C.; Rostasy, F.S. Strength of concrete subjected to high temperature and biaxial stress: Experiments and modelling. *Mater. Struct.* **1995**, *28*, 575–581. [CrossRef]
16. Wahid, N.; Stratford, T.; Bisby, L.A. Calibration of concrete damage plasticity model parameters for high temperature modelling of reinforced concrete flat slabs in fire. In Proceedings of the Applications of Structural Fire Engineering 2019 (ASFE'19), Singapore, 13–14 June 2019; Available online: https://www.researchgate.net/publication/333902896_CALIBRATION_OF_CONCRETE_DAMAGE_PLASTICITY_MODEL_PARAMETERS_FOR_HIGH_TEMPERATURE_MODELLING_OF_REINFORCED_CONCRETE_FLAT_SLABS_IN_FIRE (accessed on 29 April 2024).
17. Chang, Z.; Bradford, M.; Gilbert, R. Short-term behaviour of shallow thin-walled concrete dome under uniform external pressure. *Thin Walled Struct.* **2011**, *49*, 112–120. [CrossRef]
18. Lo Monte, F.; Kalaba, N.; Bamonte, P. On the extension of a plastic-damage model to high temperature and fire. In Proceedings of the 2nd International Fire Safety Symposium, Naples, Italy, 7–9 June 2017; Available online: https://www.irbnet.de/daten/iconda/CIB_DC31949.pdf (accessed on 29 April 2024).
19. Allam, S.M.; Shoukry, M.S.; Rashad, G.E.; Hassan, A.S. Evaluation of tension stiffening effect on the crack width calculation of flexural R.C. members. *Alex. Eng. J.* **2013**, *52*, 163–173. [CrossRef]
20. Behbahani, A.E.; Barros, J.A.O.; Ventura-Gouveia, A. Plastic-damage smeared crack model to simulate the behaviour of structures made by cement based materials. *Int. J. Solids Struct.* **2015**, *73*, 20–40. [CrossRef]
21. Hafezolghorani, M.; Hejazi, F.; Vaghei, R.; Jaafar, M.S.B.; Karimzade, K. Simplified Damage Plasticity Model for Concrete. *Struct. Eng. Int.* **2017**, *1*, 68–78. [CrossRef]